Measurement of Electrical Coupling Between Cardiac Ablation Catheters and Tissue

D. Curtis Deno*, *Member, IEEE*, Haris J. Sih, Stephan P. Miller, Liane R. Teplitsky, and Russ Kuenzi

***Abstract*—Managing cardiac arrhythmias with catheter ablation requires positioning electrodes in contact with myocardial tissue. Objective measures to assess contact and effective coupling of ablation energy are sought. An electrical coupling index (ECI) was devised using complex impedance at 20 kHz to perform in the presence of RF ablation and deliver information about electrical interactions between the tip electrode and its adjacent environment. ECI was derived and compared with clinical judgment, pacing threshold, electrogram amplitude, and ablation lesion depth and transmurality in a porcine model. ECI was also compared with force and displacement using ex vivo bovine myocardial muscle. Mean noncontact ECI was 97.2 ± 14.3 and increased to 145.2 ± 33.6 ($p < 0.001$) in clinician assessed (CLIN) moderate contact. ECI significantly improved CLIN's prediction of the variance in pacing threshold from 48.7% to 56.8% ($p < 0.001$). ECI was indicative of contact force under conditions of smooth myocardium. Transmural lesions were associated with higher pre-RF (109 ± 17 versus 149 ± 25, $p < 0.001$) and during-RF (82 ± 9 versus 101 ± 17, $p < 0.001$) ECI levels. ECI is a tip specific, robust, correlate with contact and ablation efficacy, and can potentially add to clinical interpretation of electrical coupling during electrophysiology procedures.**

***Index Terms*—Biomedical electronics, cardiac electrophysiology (EP), catheters, electrodes, impedance measurement, sensors.**

I. Introduction

CARDIAC electrophysiology (EP) procedures require catheters and electrodes to be placed in contact with the heart to diagnose and treat arrhythmias. Electrode-tissue contact is particularly vital in catheter ablation procedures where a target must be identified and thermal energy such as radio frequency (RF) is applied to selectively destroy arrhythmogenic areas of the heart. For some such procedures, the lifetime success rate of RF ablation therapy is as high as 96% [1]. For others such as persistent atrial fibrillation, six months to two-year success rates range from 50–75% [2], [3]. Electrode-tissue contact is known to be a contributing factor [4] and monitoring technologies such as force sensing catheters are being investigated to help improve outcomes [5]–[9].

It is difficult to accurately assess the quality of contact between an ablating electrode and myocardial tissue [5]–[10]. Contact is assessed today with a combination of fluoroscopic and ultrasound imaging, electrogram amplitude, RF generator reported impedance, pacing threshold (abbreviated PACE), as well as catheter manipulation history and tactile feedback. Each of these methods has its limitations including insufficient soft tissue contrast, view plane adequacy, directional electrode pairs, myocardial inhomogeneities, and friction and reaction forces.

Sensing technologies were recently introduced with the potential for more objective and applicable measures of effective contact. The force experienced by a catheter as it touches and begins to deform the endocardial surface may be sensed by small deflections of the catheter tip and transduced by an optical [6], [7] or magnetic [8] sensor into a directional contact force. This technology addresses mechanical aspects of contact with application to limiting force and hence minimizing the uncommon but significant complication of perforation. Recent studies suggest monitoring force can also lead to more consistent ablation lesions [6]–[9].

Alternatively, one may monitor complex electrical impedance to estimate physical contact with tissue [11] as well as lesion size [12]. Closely related to these applications, impedance may be used to track the degree to which ablation current may dissipate energy in adjacent tissue, thereby determining the level of electrical contact or coupling between an ablation tip electrode and its immediate surroundings. This was achieved through the use of an electrical coupling index (ECI) derived from complex impedance and said to be specific to the catheter's tip-to-tissue interface. Initially reported in human subjects [13] and in a porcine thigh muscle model [14], ECI was hypothesized to better reflect the transfer of electrical energy from catheter to tissue, and may thus be a more useful metric for RF energy ablation efficacy than measures of mechanical contact. These descriptions invite a greater exposition of ECI technology including a definition and the validation studies it depends upon. In this study, impedance measurement principles will be applied to ablation catheter tip electrodes and related to RF lesion creation. Thigh model lesion depth information will be expanded upon by *ex vivo* beef heart studies of contact angle, force, and depth. Finally, results will be provided addressing the derivation of ECI from impedance measurements, the role of cutaneous electrodes, and the influence of RF ablation on ECI in live subjects.

Manuscript received August 17, 2012; revised December 4, 2012, April 5, 2013, July 10, 2013, September 2, 2013, and October 21, 2013; accepted October 23, 2013. Date of publication November 6, 2013; date of current version February 14, 2014. This work was supported by St. Jude Medical, Cardiovascular and Ablation Technologies Division, St. Paul MN. *Asterisk indicates corresponding author.*

*D. C. Deno is with the St. Jude Medical, Cardiovascular and Ablation Technologies Division, One St. Jude Medical Drive, St. Paul, MN 55117-9913 USA (e-mail: cdeno@sjm.com).

H. J. Sih, S. P. Miller, and L. R. Teplitsky are with the St. Jude Medical, Cardiovascular and Ablation Technologies Division, One St. Jude Medical Drive, St. Paul, MN 55117-9913 USA (e-mail: hsih@sjm.com; smiller02@sjm.com; lteplitsky@sjm.com).

R. Kuenzi was with the St. Jude Medical, Cardiovascular and Ablation Technologies Division, One St. Jude Medical Drive, St. Paul, MN 55117-9913 USA (e-mail: rkuenzi@sjm.com).

Digital Object Identifier 10.1109/TBME.2013.2289328

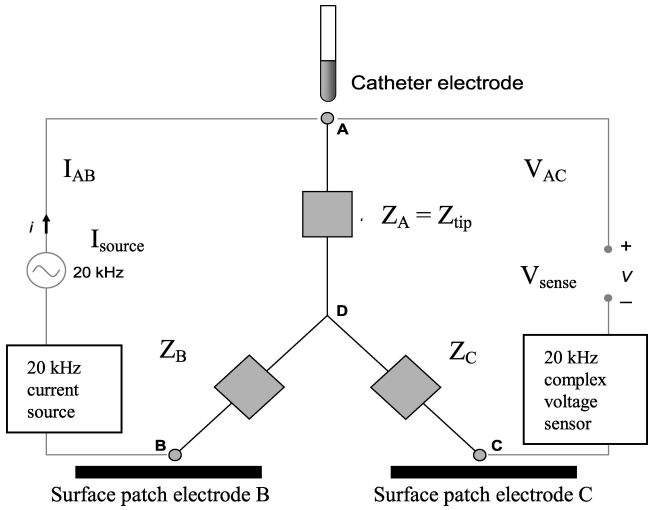

Fig. 1. Complex circuit models in the three-terminal case reduce to a delta or a Y-model equivalent circuit. A 20-kHz current I_{AB} is passed between the catheter tip (electrode A) and surface patch electrode B while simultaneously measuring voltage from the tip to surface electrode C. The voltage measurement V_{AC} accomplished without significant current flow thus measures the voltage resulting across the impedance element associated with only the tip electrode Z_A. Thus, $Z_{\mathrm{tip}} = Z_A = V_{\mathrm{AC}}/I_{\mathrm{AB}}$. Common junction D is a virtual node that corresponds to the effective boundary of measurement between A and D since $V_{\mathrm{AC}} = V_{\mathrm{AD}}$.

II. Methods

Electrical coupling measurement technology was designed for use in a clinical electrophysiology setting and so was evaluated in whole animal models. However, the measurement of variables such as contact angle and force required saline bench and thigh model animal experiments to characterize variables associated with using three-terminal complex impedance and ECI as a measure of electrical coupling.

Minitab 16.1 (Minitab Inc., State College PA) was used for statistical tests. Unless otherwise stated, the mean $\pm$ standard deviation of quantities is provided. Adjusted R^2 was used when making evaluations based on the number of independent variables. $P < 0.05$ was considered statistically significant.

A. Instrumentation Methods and Results

In human EP labs, RF current is delivered between the catheter tip and a return electrode on the body surface, and a corresponding two-terminal impedance is simultaneously measured. In the ECI measurement system, a three-terminal impedance configuration selectively measures the complex impedance between the ablation catheter tip electrode and its immediate environment. Fig. 1 shows the Y-model equivalent circuit for this three-terminal biologic impedance measurement. This model is electrically equivalent to a three-terminal circuit of arbitrary complexity under the assumption of linearity at the frequency and amplitudes of measurement.

Referring to Fig. 1, the ablation catheter tip electrode (node A) and body-surface patch electrodes (nodes B and C) are the three accessible terminals. Z_A, Z_B, and Z_C are the complex impedances of each leg of the Y-model. Node D is a virtual node that may be identified with a physical surface through the volume conductor passing between electrodes A and B and intersecting electrode C. Patch electrode location affects virtual node location and thus the spatial specificity of $Z_A = Z_{\mathrm{tip}}$. In the limit, as patch electrode separation is reduced, this becomes a two-terminal measurement reflecting the sum of Z_A and the conjoined (parallel) Z_B and Z_C. Since catheter electrode-to-electrode impedance varies little with separation until electrodes are closer than a few millimeters, catheter electrode impedance primarily reflects a region within a few millimeters of the catheter electrode's surface. As a result, with appropriately wide placement of the body-surface electrodes, Z_{tip} should reflect the impedance between the ablating electrode and its nearby environment.

To measure complex impedance, electronic circuits resolve the in-phase and quadrature components of sensed voltage. The 20-kHz frequency was chosen to limit interference with other signals in human EP labs as well as to be robust to cabling connections. Upon passing a 20 kHz, 100-μA rms current between nodes A and B (I_{AB}), voltage is measured between nodes A and C (V_{AC}). This voltage measurement, accomplished without significant current flow, measures the impedance of element $Z_A = Z_{\mathrm{tip}}$. Resistance R is determined as the ratio of in-phase voltage to current and reactance (X) as the ratio of quadrature voltage to current. Written in conventional phasor notation as a complex number, $Z_A = R_A + iX_A$, where $i = \sqrt{-1}$. For convenience, we will often omit the subscript A as this is generally the impedance of interest and use either Cartesian $Z = (R, X)$ or polar $Z = (|Z|, \angle Z)$ coordinate representations of complex impedance.

A diagram of the circuitry used to monitor three-terminal complex impedance is shown in Fig. 2(a), where the input V_{sense} appears to the left and the output I_{source} at the upper right. Precision sinusoid synthesizers operate the current source and quadrature voltage analysis functions. The 20-kHz current source's phase, adjusted in 0.1° increments, compensates for phase delays from the synthesizer to the current source output and from the voltage sensing electrodes through the amplifiers and filters to the input of the in-phase and quadrature multipliers. Precision resistor and capacitor networks were used for calibration of gains, phase, and offset compensation as well as stability assessments. The hardware's nominal operating region was $\pm$400-Ω resistance as well as reactance, producing R and X signals in the range of $\pm$5 V. Overvoltage protection and electrical isolation allowed compatibility with EP lab instrumentation and procedures. Including 1-kHz A/D conversion, LSB resolution was 0.03 Ω and electronic noise (dc to 25 Hz) was 0.04-Ω rms.

Additionally, the system needed to function in the presence of high-amplitude RF interference seen during ablation procedures (e.g., 500 kHz, 100 V). This was accomplished by a combination of passive RF attenuation, differential amplification, bandpass filtering, and quadrature demodulation as in Fig. 2(a). To ensure that the RF generator does not shunt a significant amount of 20-kHz current, *LC* blocking filters inline with the catheter electrode and the dispersive return electrode were used. These filters were tuned to provide over 2-kΩ series impedance

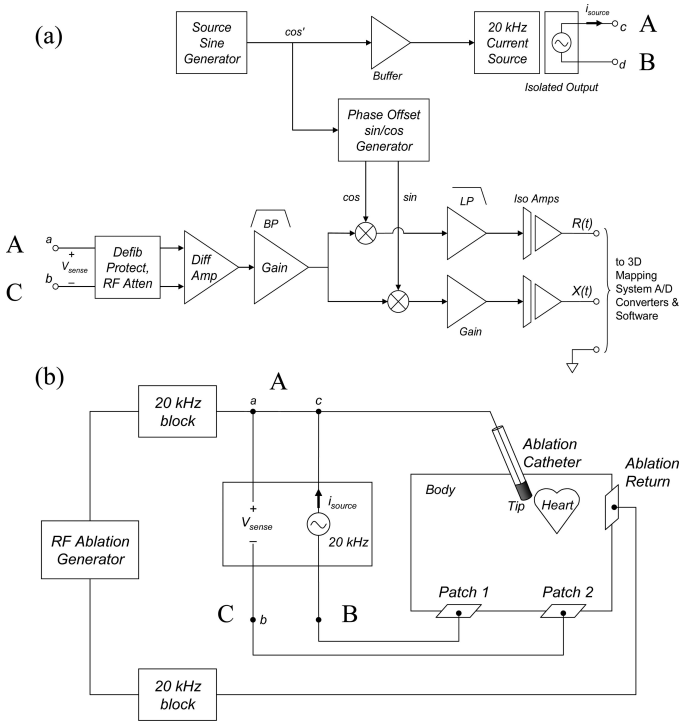

Fig. 2. Block diagram of a complex impedance measurement system. An adjustable phase precision synthesizer feeds a current source to nodes/electrodes A and B and voltage is sensed across A and C. After passive RF attenuation, differential amplification, active filtering, and analog multiplication by in-phase and quadrature precision synthesizers, the resulting signals are low pass filtered to 25 Hz, amplified, and sampled with an isolated AD converter. 20-kHz blocking filters inline with the RF ablation generator prevent significant current shunting.

at 20 kHz while adding negligible additional impedance ($<$ 1–2 Ω) to delivered RF or electrogram signals. A diagram of the resulting system appears in Fig. 2(b).

Accuracy and measurement stability was tested on each of ten days following a single initial calibration but with different cables and connections to simulate expected variations with use. Using a 100-Ω resistor, the complex impedance is ideally $Z = [+100, 0]$. The mean reported impedance was $[(99.9 \pm 1.4), (0.9 \pm 1.1)]$. Using an 80-nF capacitor, complex impedance was ideally $Z = [0, -99.5]$ compared to the reported value of $[(1.9 \pm 1.8), (-101.3 \pm 0.7)]$. Using a large capacitor, 99 μF, complex impedance was ideally $Z = [0, -0.1]$ compared to the reported value of $[(-0.8 \pm 1.5), (-0.8 \pm 0.4)]$. Absolute inaccuracies of 1–2 Ω in either R or X may, thus, occur under representative conditions. Stability over time was also assessed by *RC* networks. Over an interval of 6 h continuous use with the same cables, both R and X drifted by $[(0.4 \pm 0.5), (0.3 \pm 0.5)]$ Ω.

Finally, performance under RF was evaluated because ablation RF is a very large interfering signal and the generator is poised to shunt or load down impedance measurements of the ablation catheter's tip electrode. Low inductance, precision power resistors were employed as loads because they do not vary substantially with temperature and have virtually no reactance. As seen in Table I, RF over 0–40 W resulted in artifactual resistance changes of under 0.3 Ω and up to 0.7-Ω reactance, modest compared to the 1-Ω resolution of most RF ablation generators.

TABLE I
MEASURED IMPEDANCES OF 131 Ω POWER RESISTOR IN PRESENCE OF RF ABLATION

	Ideal	RF Power (W)				
		0	1	10	20	40
3-Term R (ohms)	131	130.57	130.29	130.51	130.52	130.67
3-Term X (ohms)	0	-0.77	-0.59	-0.34	-0.23	-0.03
RF Gen |Z| (ohms)	131	-	126	136	137	138

B. Intact Heart Models

ECI was evaluated in intact animals during clinical simulations using the 20 kHz, 100 μA three-terminal measurement described in Figs. 1 and 2. Nine swine (59.7 $\pm$ 3.1 kg) were anesthetized and placed on a ventilator in a dorsal recumbent position. From the right femoral vein a 7-Fr irrigated ablation catheter with a 4-mm tip (Cool Path$^{\mathrm{TM}}$ Ablation Catheter, St. Jude Medical, St. Paul, MN) was fluoroscopically guided to the right atrium or to the left atrium after transseptal access. Resistive and reactive components of Z_{tip} were sampled at 1 kHz simultaneously with surface ECG, bipolar atrial electrograms, and arterial blood pressure using a data acquisition system (MP150, BIOPAC Systems Inc., Goleta, CA). Modifications to an RF ablation generator (1500 T9-CP Cardiac Ablation Generator, St. Jude Medical, St. Paul, MN) also permitted the simultaneous high-fidelity acquisition of ablation generator reported temperature, impedance, and RF power. Average values over 5-s intervals were reported. Since the respiratory rate was approximately 12 breaths/min, this interval averaged out both ventilatory and cardiac fluctuations. The flow rate of room temperature saline irrigation increased from 2 to 17 ml/min upon application of RF.

Multiple surface electrodes were positioned on each animal for impedance measurements. On the animal's left lateral thorax, a 90.5 cm^2 surface electrode (Covidien E7506, Boulder, CO) was placed approximately 2 cm away from a 40.25 cm^2 surface electrode and 10 cm away from a second 40.25 cm^2 surface electrode (Covidien Uni-Patch$^{\mathrm{TM}}$ Electrode, Wabasha, MN). On the animal's right lateral thorax, a 90.5 cm^2 surface electrode (Uni-Patch, Wabasha, MN) was placed approximately 2 cm away from a 129 cm^2 surface electrode (3M, St. Paul, MN). To evaluate the three-terminal model, the catheter tip and various pairs of these surface electrodes were used as the three terminals. An ablation return electrode was placed on the dorsal thigh.

Animal studies were approved by an Institutional Animal Care and Use Committee, and studies conformed to the guide for the care and use of laboratory animals.

1) Three-Terminal Model Characterization: Several measurements and catheter maneuvers were performed to verify the three-terminal model: 1) comparing Z_{tip} obtained by three-terminal measurement to that derived from multiple two-terminal impedances measurements, 2) assessing effects of body-surface electrode position on Z_{tip}, and 3) evaluating *in vivo* stability of Z_{tip} over time.

To validate the three-terminal model and measurement apparatus, the three-terminal direct measurement of Z_{tip} was compared to Z_{tip} derived from multiple two-terminal impedance measures. Specifically, the measurement instrument of Fig. 2

was configured for both 2-terminal $(A, B = C)$ and 3-terminal (A, B, C) terminal measurements of impedance. Note from Fig. 1 that the measured impedance between any two terminals (for instance, Z_{AB} measured between terminals A and B) is equal to the sum of the impedances of the two involved legs of the circuit (in this case Z_{tip} and Z_B). Z_{tip} then can be either measured using the three-terminal model approach, or derived from the three possible two-terminal impedances

$$Z_A = Z_{\mathrm{tip}} = 1/2\left(Z_{\mathrm{AB}} + Z_{\mathrm{AC}} - Z_{\mathrm{BC}}\right). \tag{1}$$

Using subjectively assessed contact levels by the catheter operator, measurements were taken when the catheter was positioned in "noncontact" or "moderate contact" with the endocardial surface. In each animal, the direct three-terminal measurement of Z_{tip} was compared to the derived Z_{tip} from three two-terminal measurements. Patch associated impedances Z_B and Z_C were also derived in a similar manner from linear combinations of Z_{AB}, Z_{AC}, and Z_{BC}.

2) Electrode Location: For clinical applications, suitable body surface electrode locations needed to be defined. To investigate the effect of surface patch electrode location, four configurations were tested. Surface electrodes were either adjacently spaced (2 cm), closely spaced (10 cm), or placed on contralateral sides of the thorax (about 30 cm apart). The limiting case of a single common electrode was also included. Empiric three-terminal measurements of Z_{tip} were then compared to those derived from two-terminal measurements as in (1).

3) Stability and Sensitivity: An electrophysiology study may last several hours during which measurements taken by the instrumentation should be stable. To evaluate clinical case stability, three-terminal measurements were evaluated over the course of each animal study. Complex impedances in similar noncontact locations were compared at the beginning and end of each multihour animal study. To evaluate sensitivity to cutaneous electrode changes, a 36.5-Ω resistor was inserted in series with 129 and 40 cm^2 cutaneous electrodes and the resulting changes of impedance and ECI were observed.

4) ECI Derived: After obtaining the complex impedance, a single, real-valued metric was sought, which could be displayed and quantified during clinical electrophysiology cases. Preliminary *in vivo* data indicated that both R and X were responsive to tissue contact or coupling. Affine combinations of R and X were sought to arrive at a formula for ECI

$$\mathrm{ECI}\,(t) = a\,R\,(t) + b\,X\,(t) + c. \tag{2}$$

Coefficients a, b, and c were determined from measurements of Z_{tip} in the absence of RF according to criteria in the next section. ECI defined this way immediately reflects cardiac and ventilatory variations.

5) Validation and Ablation: ECI was also validated under clinically relevant conditions. Z_{tip} was measured when the catheter was placed in different levels of contact as might be encountered in an EP procedure. An experienced catheter operator (clinician) placed the catheter in contact with the atrial endocardium at the subjectively assessed levels of "none," "light," "moderate," and "firm." To assess these levels, the clinician used a combination of fluoroscopic images, bipolar atrial electrogram amplitudes (AEGMs), experience with manipulation and tactile feel, and 3-D catheter position information from a catheter navigation system (EnSite Velocity$^{\mathrm{TM}}$ Cardiac Mapping System, St. Jude Medical, St. Paul, MN). The clinician was coached to associate a "moderate" level of contact with typical and good contact for the purposes of mapping and ablation. The operator positioned the catheter in both atria at the four different contact levels and at various locations, while complex impedance and AEGMs were recorded and PACEs assessed. PACEs were determined using an EP-3 stimulator (St. Jude Medical, West Berlin, NJ) using 1 ms duration current pulses by a standardized technique. If pacing capture could not be achieved at the maximum output of the stimulator (20 mA), the threshold was conservatively defined to be 25 mA for analysis.

To assess the possible clinical value of ECI, regression analysis was performed relative to PACEs. PACEs were considered the objective standard for assessing the degree of electrical coupling in healthy atrial tissue. As the PACE distribution was asymmetric, the logarithm of the PACE was calculated to normalize the distribution. To perform the multiple regression analysis, the four levels of clinician assessed contact (CLIN) were assigned numeric values (0 = none, 1 = light, 2 = moderate, and 3 = firm). These contact levels along with R and X were then used to predict the logarithm of the PACEs. Analyses of variance were used to determine if adding R and X information to CLIN, the clinician's subjective assessment of contact, improved prediction of PACEs. Atrial electrogram signal amplitude (AEGM) was also employed and correlations examined between AEGM, PACE, CLIN, and ECI.

Linear regression techniques were used to derive the specific formulation for ECI in (2). Since ECI is an original index of electrical coupling, we were free to choose its scale. We did so by fixing $c = 0$ and using R and X alone and in combination to predict the log of PACE. The best fit to PACE and statistically significant set of coefficients provided the formula for ECI.

Finally, to assess the performance of ECI with RF ablation, 54 ablation applications at 20 and 40 W for 40 s in either the left or right atrium were created while temperature, electrograms, and ECI were monitored. The catheter was held in a stable location at a constant level of contact for at least 5 s before, during, and at least 10 s after ablation. Recorded signals from a noncontact location were used as controls. Numeric results were obtained from 5-s windows immediately before starting RF and during the last 5 s of RF. Lesion transmurality and depth at necropsy was used to assess the observed ECI changes.

C. Bench Test Methods

Once ECI was defined, it could be evaluated with controlled Wetlab bench testing to quantitatively explore correlations of ECI to applied force between the catheter and tissue, the depth of penetration into tissue, and the dependence of ECI on the angle of contact between the catheter and tissue. For these characterizations, complex impedance was measured and ECI computed on sections of freshly excised bovine heart. Ventricular tissue was sectioned in 1.5–2-cm slabs to create a uniform tis-

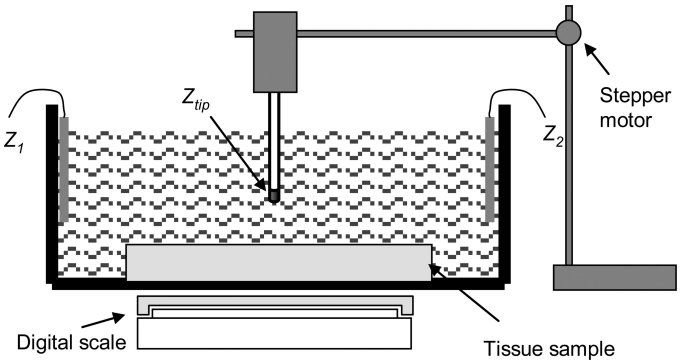

Fig. 3. Setup for bench model experiments. Freshly excised beef heart tissue was submerged in 20 C saline. Force, vertical displacement, as well as complex impedance and ECI were measured as an ablation catheter tip approached and entered into heart tissue. The 90° angle of contact is shown.

sue surface and was placed in a Pyrex chamber filled with a 20 C mixture of saline and water to a blood-like conductivity of 6.2–6.8 mS/cm. Two large electrodes placed on either side of the beef heart section were used for the three-terminal measurements. An irrigated ablation catheter with a 4-mm tip (7-Fr Cool Path Ablation Catheter, St. Jude Medical, St. Paul, MN) was mounted on a motorized fixture and lowered into the tank to make contact with the tissue. The chamber was placed on a digital scale (Ohaus, Pine Brook, NJ) to measure the applied force, expressed per convention in grams. Data acquisition as well as control of the stepper motor was through a custom LabVIEW program and commercial data acquisition hardware (National Instruments, Austin, TX) as shown in Fig. 3.

To characterize the relationship between ECI, distance, and applied force, the catheter was moved downward to the tissue. A stepper motor controlled the vertical displacement of the catheter during force and complex impedance measurements. Displacement, starting at 1 cm above the smooth myocardial surface, continued to a depth of 4 mm below the tissue surface in 0.1-mm increments. To characterize the effect of angle of contact, the catheter was placed in a bracket to hold the catheter at 0, 30, 60, or 90° relative to the beef heart surface. For the purposes of testing for angular dependence, contact was defined to be 2 g of force and noncontact was 0-g force at 10 mm above the tissue surface.

III. Results

A. Intact Heart Results

Using the three-terminal "Y"-model, $Z_{\rm tip}$ was both directly measured and calculated with the catheter in the atria. Measurements were taken with the catheter in different levels of endocardial contact 1) to confirm the three-terminal model measurements against standard two-terminal impedance measurements, 2) to determine the sensitivity of the three-terminal model to different surface electrode configurations, 3) to establish the stability of the measurement system over time, and 4) to verify the ability of ECI to reflect contact in a realistic model of clinical electrophysiology catheterization procedures.

TABLE II
Comparison of Tip (Z_{tip}) and Cutaneous Patch (Z_B, Z_C) Electrode Impedances Measured In Vivo Under Conditions of Contact and Noncontact and by 2- and 3-Terminal Measurements

		Non-contact	Contact
3-terminal direct measurement			
Z_{tip} 0.29 cm^2	R (Ω)	82.0 ± 5.3	116.5 ± 12.6
	X (Ω)	–3.9 ± 1.0	–6.1 ± 1.5
	ECI	101.7 ± 4.9	147.4 ± 11.2
Y-model elements derived using Equation 1			
Z_{tip} 0.29 cm^2	R (Ω)	84.0 ± 5.4	117.9 ± 12.1
	X (Ω)	–3.0 ± 1.1	–5.1 ± 1.6
	ECI	99.4 ± 4.8	143.8 ± 11.0
Z_B 129 cm^2	R (Ω)	25.5 ± 4.1	25.0 ± 4.3
	X (Ω)	–31.4 ± 10.9	–31.0 ± 10.8
Z_C 40 cm^2	R (Ω)	79.8 ± 23.6	80.6 ± 23.6
	X (Ω)	–67.5 ± 14.8	–67.5 ± 14.9

TABLE III
Effect of Cutaneous Patch Electrode Separation on Tip Electrode Resistance, Reactance, and ECI in Noncontact Condition

Cutaneous Configuration	Z_{tip}, Tip Impedance		ECI
	R (Ω)	X (Ω)	
Contralateral (30 cm)	82.0±5.4	–3.8±1.0	99.4±4.8
Close (10 cm)	87.7±3.6	–4.9±0.9	105.3±2.5
Adjacent (2 cm)	101.4±7.6	–11.4±3.5	160.4±16.6
Common (0 cm)	108.4±6.7	–35.8±10.2	290.9±51.2

1) Three-Terminal Model Characterization: With the catheter tip stable in either a noncontact location or in moderate contact with the atrial endocardium, three-terminal measurements of $Z_{\rm tip}$ were compared to the calculated $Z_{\rm tip}$ from two-terminal impedance measurements using (1) and Fig. 1. Although not quite simultaneous, two- and three-terminal methods to determine $Z_{\rm tip}$ agree well, resulting in values within 1–2 Ω as seen in the top half of Table II (for example 82.0 versus 84.0 and -3.9 versus -3.0 Ω under noncontact). As expected, the larger patch electrode (Z_B, 129 $\rm cm^2$) had consistently lower resistance and capacitive reactance than the smaller patch electrode (Z_C, 40 $\rm cm^2$). Importantly, the two levels of contact influenced both $Z_{\rm tip}$ components and ECI, but did not change patch electrode associated impedances Z_B or Z_C, arguing for tip electrode specificity of $Z_{\rm tip}$ and ECI to electrode-tissue contact or coupling.

The intracardiac tip electrode was distinctive. With a surface area of 0.29 $\rm cm^2$, it exhibited the least negative reactance, indicative of a much greater effective capacitance.

2) Electrode Location: Three-terminal measurements of tip impedance were made for three different cutaneous electrode configurations with the catheter in the same stable noncontact location. As seen in Table III, as cutaneous electrode spacing decreased (from "Contralateral" to "Close," "Adjacent," and "Common" spacing), resistance R, capacitive reactance $-X$, and ECI all increased reflecting increasing contributions from the cutaneous patches. The dramatic change in reactance with

cutaneous electrode separation emphasizes that surface electrodes possess significant reactance, consistent with model results from Table II. Among the configurations tested, Contralateral positioning yielded the lowest values and thus presumably the most tip selective values of $Z_{\rm tip}$ and ECI.

3) Stability and Sensitivity: Three-terminal impedance measurements were made in a noncontact location at the start and end of each animal's study to assess the measurement stability. Despite the fact that the observations are separated by 6.3 $\pm$ 2.2 h, and despite slightly different noncontact locations from the initial to the final measurements, changes in $Z_{\rm tip}, Z_B$, and Z_C remained less than 10 Ω. The mean absolute value of change in $Z_{\rm tip}$ was 3.9 $\pm$ 3.4 Ω in resistance and 0.7 $\pm$ 0.5 Ω in reactance. While there was a statistically significant decrease in ECI by -5.6 ± 5.4 units ($p = 0.031$), the mean change was only 5.8 $\pm$ 5.6% suggesting a stable measurement system over long and clinically relevant durations.

Sensitivity to changes of cutaneous electrode impedance was assessed by placing an additional 36.5-Ω resistance in series with these electrodes. The mean change of tip impedance was $[(0.03 \pm 0.20), (0.03 \pm 0.05)]$ and $[(0.02 \pm 0.20), (0.03 \pm 0.05)]$ ohms using nodes B and C, respectively. This amounted to a negligible change of ECI of -0.07 ± 0.32 and -0.10 ± 0.34 units, respectively.

4) ECI Derived: A scalar index derived from R and X was sought that predicted the electrical coupling between an ablation catheter's tip and its surroundings. PACEs in healthy atrial myocardium were treated as an objective standard for the electrical coupling level in healthy and relatively homogeneous atrial tissue since they are indicative of electrical interaction of tip to tissue and since they are not directionally sensitive as are bipolar AEGM signal amplitudes. Throughout tests involving pacing, both R and X signals were monitored without detectable artifact. Although characteristic changes occurred with variations of electrode-tissue contact, the magnitude of and changes in reactance, X, in $Z_{\rm tip}$ were smaller than those of resistance R.

To determine an appropriate weighting in a simple formula, a regression analysis of R and X relative to PACE was performed. From 300 observations made over all nine animals, the best prediction of PACE was obtained by weighting reactance 5.1 times as much as resistance

$$\text{ECI}\,(t) = R\,(t) - 5.1\ \ X\,(t)\,. \tag{3}$$

This regression of R and X on PACE alone accounted for 48.9% of the variability in PACE as indicated by the adjusted-R^2. The regression also revealed that this specific combination was statistically superior to R or X alone ($p < 0.001$) and to impedance magnitude $|Z| = \sqrt{R^2 + X^2}$ or phase $\angle Z = \text{atan2}(X, R)$ alone (both $p < 0.001$).

Prediction of PACE by the clinician assessed contact levels yielded an adjusted-R^2 of 48.7%, very nearly the same as the ECI-based assessment with R^2 of 48.9%. Combining the clinician assessed contact levels with ECI in a regression yielded a modest but significantly greater adjusted-R^2 of 56.8% ($p < 0.001$), implying that ECI may improve a clinician's ability to predict electrical coupling.

TABLE IV
R^2 CORRELATIONS OF RF GENERATOR IMPEDANCE, TIP ELECTRODE R, X, AND ECI SIGNALS TO EACH OTHER

Variable	RF Gen |Z|	3-Term R	3-Term X	ECI
RF Gen |Z|	1	0.96	0.27	0.75
3-Term R	0.96	1	0.35	0.83
3-Term X	0.27	0.35	1	0.76
ECI	0.75	0.83	0.76	1

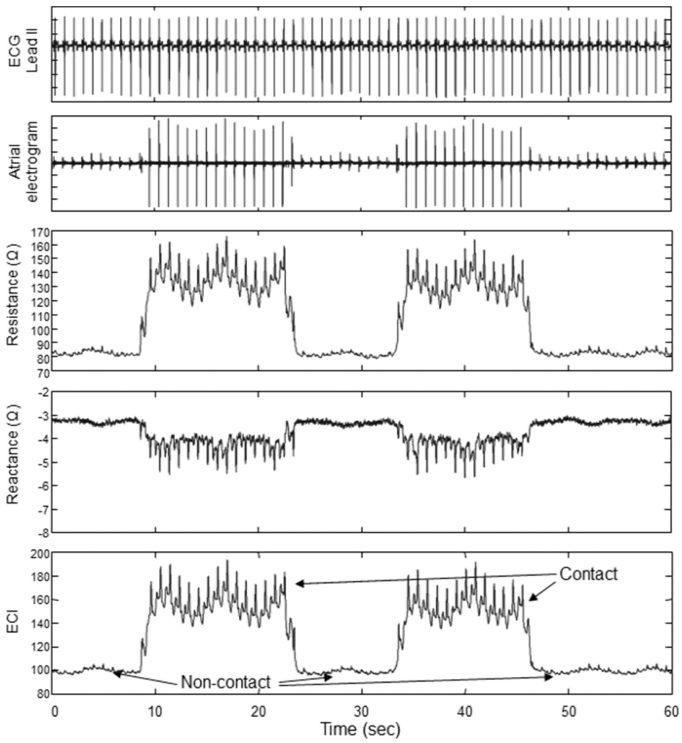

Fig. 4. A selected example of signals as the catheter moves from non-contact to contact locations. In addition to changes in mean levels, resistance, reactance, and ECI vary with respiratory and cardiac cycles, especially prominently during contact.

Additional evidence supporting including both components of complex impedance, R and X, in an index of electrical coupling was derived from assessments of similarity to each other and to RF generator reported impedance. Signal variation over 3-min intervals consisting of multiple cardiac and ventilatory cycles as well as contact and noncontact conditions revealed generator impedance $|Z|$ and three-terminal resistance R to be similar (R^2 values of 0.96) but that reactance X was relatively independent (R^2 values of 0.27–0.35) of R and generator $|Z|$ as seen in Table IV's list of pairwise R^2 values.

5) Validation and Ablation: ECI was monitored during clinical catheter manipulations. In the most basic maneuver, the catheter operator alternated between noncontact and moderate contact locations with the atrial endocardium. A selected example of $Z_{\rm tip}$ and ECI signals is seen in Fig. 4, where PACE and multiple C-arm fluoro views were employed for additional certainty. All indices including clinician assessed contact mirror the impedance and ECI changes from noncontact to contact. Mechanical ventilation and cardiac fluctuations may also be seen.

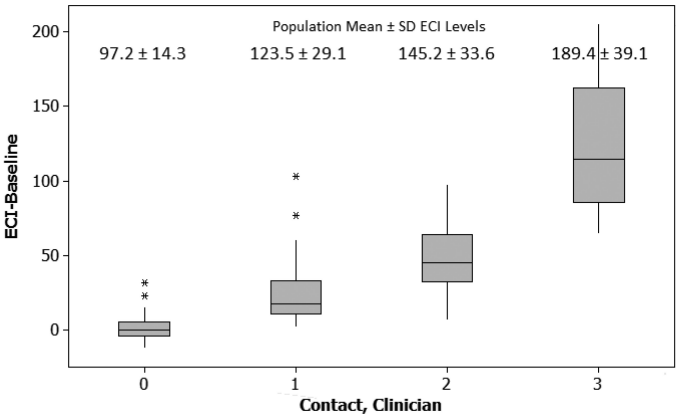

Fig. 5. ECI values stratified by clinician assessed level of contact. Both changes from each subject's baseline (Boxplot) and population means (numbers) reveal statistically significant agreement between electrical coupling and clinician assessed contact.

To more broadly characterize changes of ECI as a result of clinician assessed moderate contact, data were pooled from all nine swine and 741 observations. Mean noncontact ECI was 97.2 ± 14.3 (range $= 73$–211, $n = 240$) and increased to 145.2 ± 33.6 (range $= 67$–237, $n = 322$) with contact.

This study also sought to compare indices of contact (AEGM, PACE, CLIN, and ECI) for consistency over this same large set of observations. None of the measures correlated strongly with others. Adjusted R-squared values of the six possible pairwise comparisons varied from 0.20 to 0.47. Although all correlations are significantly different from zero, the proportion of variance explained was modest. ECI was involved in the two strongest relationships ECI-PACE and ECI-CLIN with PACE and clinician assessed contact level (R^2 of 0.47 and 0.46, respectively).

Clinician assessed level of contact is an important subjective standard of comparison and was contrasted with the objective indices of PACE, AEGM, and ECI. Significance testing was conducted using an ANOVA with multiple comparisons. ECI was the only index whose population mean levels were distinct ($p < 0.001$) at each level of clinician assessed contact (see text of Fig. 5) as were ECI changes from each subject's noncontact baseline (see Boxplots of Fig. 5, $p < 0.001$).

In addition to characterizing ablation catheter tip to tissue contact, ECI was also used during RF ablation, revealing characteristic changes shown in Fig. 6. The temperature sensed reflects a balance between cool irrigation fluid and RF heating. With the application of RF and stable catheter contact, both resistance and reactance move toward zero in similar but not identical fashions. Following the completion of this lesion, the AEGM remained diminished but R, X, and ECI all partially returned to baseline, reflecting a persistent lesion-associated change in electrical properties despite temperature returning to baseline.

ECI and RF ablation applications (12 at 20 W and 42 at 40 W) were analyzed in the manner presented by Holmes *et al*. [14] to characterize depth and transmurality. Lesions were created at atrial sites of similar thickness (LA: 2.2 ± 1.1 mm ($n = 21$), RA: 3.0 ± 1.9 mm ($n = 33$), $p > 0.05$). The pre-RF, during RF, and percent change with RF values of ECI were all predictive of transmural lesions in this study as seen in Table V.

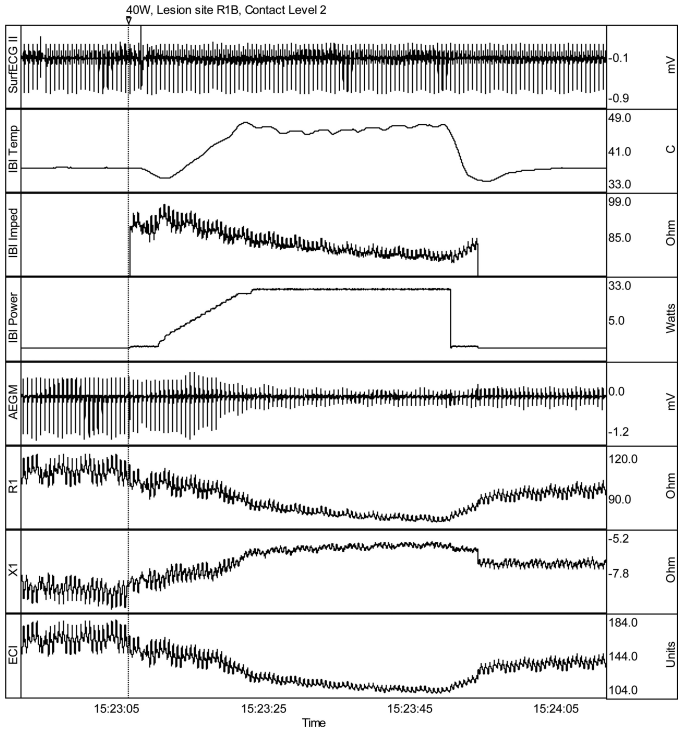

Fig. 6. Example of the application of 40-W RF while maintaining consistent contact with atrial myocardial tissue. Irrigated tip sensor temperature rises modestly as electrogram amplitude decreases and complex impedance components R1 and X1 move toward zero. In the presence of stable contact, ECI may decrease as a result of thermal effects on conductivity (about 2%/°C [15]) as well as RF induced tissue changes. Following RF, as temperature returns to baseline, a persistent change in electrical properties is noted.

TABLE V
ECI LEVELS BEFORE AND DURING RF AND RF INDUCED CHANGES IN ECI ARE ASSOCIATED WITH LESION TRANSMURALITY

Lesion Variable	ECI pre-RF	ECI during-RF	Δ↓ECI (%)	Δ↓|X| (%)
Non-transmural (n=8)	108.7 ± 17.5	81.5 ± 9.3	24.1 ± 10.0	63.6 ± 36.8
Transmural (n=46)	149.4 ± 25.4	101.3 ± 17.0	31.8 ± 6.9	62.6 ± 18.7
P-value	< 0.001	< 0.001	0.009	0.908

The substantial change in reactance, X, during RF ($62.7 \pm 21.8\%$) did not distinguish transmural lesions. The overall mean reduction in ECI ($30.6 \pm 7.4\%$) was greater in this study than the 16.6% observed by Holmes *et al*., but choosing a proportionately larger cutoff (25% reduction) also separated transmural from nontransmural lesions with a positive predictive value of 92.3% (Fisher exact test $p = 0.03$). ECI reduction >25% was also associated with greater lesion depth (1.3 ± 1.1 versus 2.8 ± 1.7 mm, $p = 0.002$).

ECI can be monitored with a 3-D mapping system during catheter manipulation and ablation. As shown in Fig. 7, ECI helped confirm an effective RF lesion in the RA by virtue of the time course shown. The ECI signal varies regularly with ventilation and cardiac cycles, gradually reduces during RF ablation, and abruptly returns almost to its baseline level. In addition, instantaneous ECI is portrayed by the color and size of an ablation catheter tip "beacon" and reported numerically.

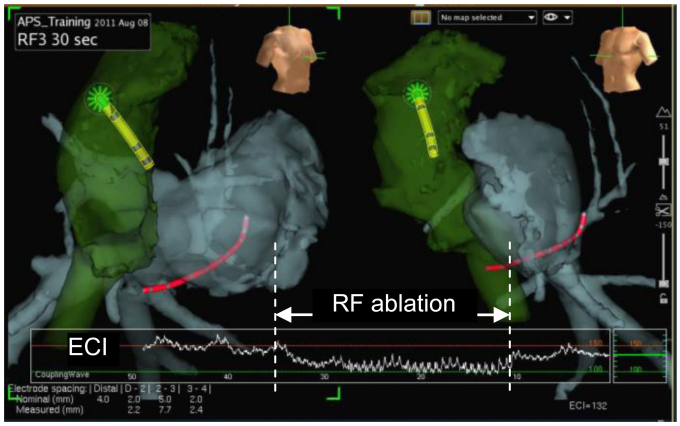

Fig. 7. Display of ECI during RF ablation at a stable location in the swine right atrium. The yellow ablation catheter is in contact with the lateral right atrium (green). In the ECI waveform window, ECI is initially high (around 150) reflecting contact with healthy atrial tissue. It then decreases with RF application and tissue heating, coming to a new steady-state level (about 110) that fairly abruptly increases to an intermediate level (130) at the conclusion of RF. A "beacon" on the catheter tip responds in size and color as ECI changes.

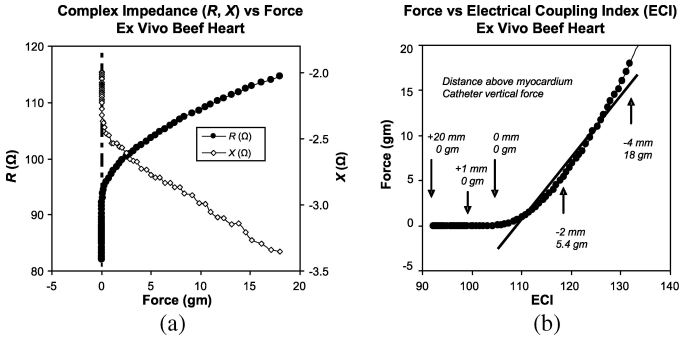

Fig. 8. Response of complex impedance and ECI to proximity and contact force in ex vivo myocardial tissue. (a) Resistance (R, filled circles) and reactance (X, open diamonds), and thus ECI, respond starting within about 2 mm of the tissue surface. (b) In the clinically relevant range of 0–20-g applied force, ECI changes nearly linearly with applied force.

B. Bench Test Results

ECI and impedance components R and X at the catheter tip varied in a manner that reflects both proximity (without physical contact) and force. Complex impedance and ECI were not sensitive to distance above the myocardial surface until the tip electrode came to within about 2 mm of the tissue surface. A representative example appears in Fig. 8 for the case where the ablation catheter is perpendicular or 90° relative to the myocardial surface. Shortly before physical contact was achieved, resistance R and capacitive reactance $-X$ began to increase. As distance from the surface went from 20 to 2 to 0 mm, ECI increased from 93 to 96 to 103, respectively. As the tip electrode was further advanced 2 mm into the tissue surface, ECI steadily increased to 118 and contact force rose to 5.4 g. Over the clinically relevant range of 0–20 g, ECI changes were nearly proportional to force (1.5 ECI units per gram force) and penetration depth.

ECI was also found insensitive to catheter-tissue contact angle when force was controlled. ANOVA analysis indicated no dependence of ECI on catheter contact angle either in contact (2-g force, 109.7 ± 10.2 ECI units, $p = 0.55$) or noncontact (66.6 ± 10.5 units, $p = 0.97$) and no significant association of ECI change (from noncontact to contact) with angles of 0–90° although accompanied by additional displacement into tissue of 1.2 ± 0.2 mm at 90°.

IV. Discussion

This paper explains how an electrode's localized complex impedance may assist with catheter ablation in a cardiac EP lab. From 20-kHz impedance signals, an electrical coupling index or ECI was defined based on *in vivo* maneuvers and PACE. ECI was shown to be distinct from RF generator reported impedance and from the subjective clinical assessment of contact. Evidence was also presented that ECI was associated with ablation lesion depth and transmurality. This study supports a role for ECI's electrode-to-tissue electrical coupling in a clinically relevant environment.

Previous studies have shown the importance of electrode contact on ablation quality [4], [5], [10], [16], [17]. Factors identified include electrode surface contact area, force, and impedance [11], [12], [18]. However, due to the difficulty in assessing contact levels *in vivo*, a standard for clinically relevant contact does not exist.

Ablation generator reported impedance at around 500 kHz has been proposed as an indicator of coagulum formation and steam pops, tissue heating, endocardial contact, lesion dimension, and as a way to assess tissue composition [11], [12], [17]–[24]. Generator impedance in some cases is only available when RF energy is applied and is susceptible to changes in skin or cutaneous electrode impedance and at 500 kHz to cable layout affecting reactance. The three-terminal impedance measurement system in Fig. 2 overcomes these limitations, allowing for a real-time assessment of electrical coupling that can be measured and displayed during RF application and cardiac pacing.

A. ECI and Electrical Coupling

Electrical coupling technology has been reported in human clinical studies of AF ablation subjects. A first Leipzig study [13] compared catheter tip contact with ECI in the same four-level manner as this report. Mean ECI levels were similar for the Leipzig human studies and our swine, 115 ± 12 versus 97 ± 14, respectively for noncontact and 144 ± 17 versus 145 ± 34 for moderate contact. ECI changes from subject specific baselines reliably predicted the clinician's distinctions between contact and noncontact. Furthermore, both this porcine and the human study [13] found ECI measurements to be fairly stable over 6.3 ± 2.2 versus 2.3 ± 0.7 h, respectively, declining slightly by 5.6 versus 9.3 ECI units or 5.8 versus 8.1%, respectively. More recently [25], pulmonary vein isolation for AF was found more successful when ECI was available compared to when it was not (58 versus 30%). ECI use may also be associated with fewer lesion gaps and faster gap closure [25].

Both the Leipzig study [13] and this one found ECI changes from a subject-specific baseline more characteristic of contact as judged by a clinician. This suggests temporal displays of ECI

(such as those of Figs. 6 and 7), where baselines can be inferred are likely to be of value.

ECI was formulated as a linear combination of resistance and reactance based on regression modeling of PACEs in nine porcines. The $R - 5.1X$ combination was superior to R or X alone or to generator reported impedance. PACE data obtained in a similar manner from human subjects, as described in [13], permitted us to validate this expression for ECI. The human subject derived expression, $R - 8.3X$, was not significantly different from $R - 5.1X$ since both expressions provided a 51% adjusted-R^2 predicting PACE from ECI and CLIN. ECI's weighting of reactance reflects the reactive component's unique information. Using an intact heart animal model, we demonstrated the localization and validity of a three-terminal electrical impedance model and ECI in both contact and noncontact situations. Complex impedance and ECI signals remained valid despite pacing or RF ablation. In addition, ECI reflected localized tip electrode changes and was robust to variations in cutaneous electrode impedance/size.

ECI was evaluated in bench studies to allow for measurements not easily controlled in a clinical environment. ECI was correlated with force and displacement on smooth surfaced myocardial tissue over the clinically relevant range of 0.1–20 g of force. However, ECI also changed just prior to physical contact with tissue, emphasizing its relation to electrical coupling and not just physical contact or mechanical force. ECI at fixed force was also observed to be essentially independent of catheter orientation with respect to myocardial tissue. These results distinguish ECI and electrical coupling from force or physical contact.

Assessments of contact and coupling are valuable for diagnostic purposes (confirming adequate electrogram sampling and affirming anatomic model completeness) as well as to help form adequate transmural ablation lesions. We speculate that ECI changes before, during, and after RF may predict, monitor, and assess lesion formation. ECI during RF reflects a number of influences including surface contact, thermal effects, and lesion associated changes from cell disruption and swelling. This study found transmural lesions associated with greater ECI levels preablation and greater ECI reduction during RF, although the latter occurred at twice the threshold suggested by Holmes *et al*. [14] in their lower power and shorter applications of RF with a prototype ablation catheter. Holmes *et al*. [14] also tested lesion formation in the perfused thigh model, where ablation power, time, and force were controlled (30 W, 60 s, and 10 g, respectively) and found lesion depth variations were related to ECI, consistent with our finding of greater depth with ECI reductions of $>25\%$. ECI may better account for variations in compliance or surface area independent of force. These data and [25] suggest that prospective human studies may find ECI to be a predictor of the thermal dose during RF ablation and thus be useful to monitor lesion progression.

ECI compared well with more traditional indices of contact or electrical coupling during catheter manipulations. In clinical practice, there is ambiguity associated with all relevant indices including the four used in this study: bipolar AEGM, PACE, clinician assessed level of contact (CLIN), and impedance-based ECI (ECI). This study found that ECI provided additional value predicting PACE compared to CLIN alone. When clinicians were blind to ECI, PACE, and AEGM, the pairwise agreement among all indices was modest with R^2 values ranging from 0.21–0.47. Traditional measures of contact are variable and in one report [26] can lead to errors in contact assessment as much as 46% of the time. This variability emphasizes the need for relevant and objective measures of contact, like force and ECI. Clinicians may have difficulty recognizing low and no contact since high PACEs or low values of ECI and AEGM were sometimes associated with nonzero clinician assessed contact.

B. Limitations

ECI is a real-time impedance derived signal that was moderately correlated with a clinician's subjective assessment of contact in the intact heart. Factors other than surface area contact influence the complex impedance, including conductivity changes due to catheter irrigation, narrow blood vessels surrounded by lung, heating during RF ablation, and residual changes after RF induced cell damage. It may be possible to further exploit changes in resistance and reactance or susceptance to separate RF induced tissue change from temperature as suggested by He *et al*. [12]. In its present form, however, ECI is pertinent to the behavior of electrical coupling—that is, the ability to deliver pacing or RF electrical energy to a region near an ablation tip electrode. For example, even without contact, electrical coupling to blood around a catheter in a pulmonary vein will increase because the vein is surrounded by resistive lung tissue, promoting localized electrical heating. Contact on the other hand implies electrical coupling. So although one may loosely regard ECI as contact, more precisely it measures electrical coupling.

Another limitations of this study is the use of pacing threshold pacing threshold in healthy atrial tissue, not thermal dissipation, as its primary measure of electrical coupling and contact. The alternative CLIN was not objective and AEGM excluded because it was among the least correlated indices and because its bipole is directionally sensitive and involves an additional catheter electrode.

C. Conclusions

ECI and a three-terminal impedance model were introduced and verified as a method for assessing electrical coupling during cardiac catheterization procedures. ECI is understood to be an index of electrical coupling related to proximity, contact force, and tissue distribution around an ablation tip electrode that is both sensitive and specific as the tip comes into proximity and contact with myocardial tissue. ECI can be evaluated in real time and integrated into a 3-D mapping system, providing dynamic feedback to the catheter operator.

In summary ECI and its three-terminal measurement is a tip specific, robust, correlate with known measures of contact and ablation efficacy, and can potentially add to clinical interpretation of electrical contact/coupling. ECI may be a marker for effective delivery of RF ablation and may be a useful metric to monitor during cardiac catheterization and ablation procedures.

ACKNOWLEDGMENT

The authors gratefully acknowledge substantial contributions to this work by the following individuals: Bob Aiken, Jim Baker, Judson Brown, Jeff Burrell, Hong Cao, Heath Carter, Jeremy Dando, Ken Drew, Dan Dwyer, Jeff Fish, Maurice Goudeau, Erik Hanson, John Hauck, Lewis Hill, Glen Kastner, Shawn McCutcheon, Saurav Paul, Harry Puryear, Jihong Qu, Brian Schmidt, Jeff Schweitzer, and Tommy Zerse.

REFERENCES

[1] L. Wang and R. Yao, "Radiofrequency catheter ablation of accessory pathway-mediated tachycardia is a safe and effective long-term therapy," *Archives Med. Res.*, vol. 34, pp. 394–398, 2003.

[2] R. Cappato, H. Calkins, S. A. Chen, W. Davies, Y. Iesaka, J. Kalman, Y. H. Kim, G. Klein, D. Packer, and A. Skanes, "Worldwide survey on the methods, efficacy, and safety of catheter ablation for human atrial fibrillation," *Circulation*, vol. 111, pp. 1100–1105, 2005.

[3] R. J. Hunter and R. J. Schilling, "Long-term outcome after catheter ablation for atrial fibrillation: Safety, efficacy and impact on prognosis," *Heart*, vol. 96, pp. 1259–1263, 2010.

[4] D. E. Haines, "Determinants of lesion size during radiofrequency catheter ablation: The role of electrode-tissue contact pressure and duration of energy delivery," *J. Cardiovasc. Electrophysiol.*, vol. 2, pp. 509–515, 1991.

[5] S. A. Strickberger, V. R. Vorperian, K. C. Man, B. D. Williamson, S. J. Kalbfleisch, C. Hasse, F. Morady, and J. J. Langberg, "Relation between impedance and endocardial contact during radiofrequency catheter ablation," *Am. Heart J.*, vol. 128, pp. 226–229, 1994.

[6] K. Yokoyama, H. Nakagawa, D. C. Shah, H. Lambert, G. Leo, N. Aeby, A. Ikeda, J. V. Pitha, T. Sharma, R. Lazzara, and W. M. Jackman, "Novel contact force sensor incorporated in irrigated radiofrequency ablation catheter predicts lesion size and incidence of steam pop and thrombus," *Circulation: Arrhythmias Electrophysiol.*, vol. 1, pp. 354–362, 2008.

[7] A. Thiagalingam, A. D'Avila, L. Foley, J. L. Guerrero, H. Lambert, G. Leo, N. Ruskin, and V. Y. Reddy, "Importance of catheter contact force during irrigated radiofrequency ablation: Evaluation in a porcine ex vivo model using a force-sensing catheter," *J. Cardiovasc. Electrophysiol.*, vol. 21, pp. 806–811, 2010.

[8] F. Perna, E. K. Heist, S. B. Danik, C. D. Barrett, J. N. Ruskin, and M. Mansour, "Assessment of catheter tip contact force resulting in cardiac perforation in swine atria using force sensing technology," *Circ. Arrhythm. Electrophysiol.*, vol. 4, pp. 218–224, 2011.

[9] D. C. Shah, H. Lambert, H. Nakagawa, A. Langenkamp, N. Aeby, and G. Leo, "Area under the real-time contact force curve (force-time integral) predicts radiofrequency lesion size in an in vitro contractile model," *J. Cardiovasc. Electrophysiol.*, vol. 21, pp. 1038–1043, 2010.

[10] F. H. M. Wittkampf and H. Nakagawa, "RF catheter ablation: Lessons on lesions," *Pacing Clin. Electrophysiol.*, vol. 29, pp. 1285–1297, 2006.

[11] H. Cao, S. Tungjitkusolmun, Y. B. Choy, J. Z. Tsai, V. R. Vorperian, and J. G. Webster, "Using electrical impedance to predict catheter-endocardial contact during RF cardiac ablation," *IEEE Trans. Biomed. Eng.*, vol. 49, no. 3, pp. 247–253, Mar. 2002.

[12] D. S. He, M. Bosnos, M. Z. Mays, and F. Marcus, "Assessment of myocardial lesion size during in vitro radio frequency catheter ablation," *IEEE Trans. Biomed. Eng.*, vol. 50, no. 6, pp. 768–776, Jun. 2003.

[13] C. Piorkowski, H. Sih, P. Sommer, S. P. Miller, T. Gaspar, L. Teplitsky, and G. Hindricks, "First in human validation of impedance-based catheter tip-to-tissue contact assessment in the left atrium," *J. Cardiovasc. Electrophysiol.*, vol. 20, pp. 1366–1373, 2009.

[14] D. Holmes, J. M. Fish, I. A. Byrd, J. D. Dando, S. J. Fowler, H. Cao, J. A. Jensen, H. A. Puryear, and L. A. Chinitz, "Contact sensing provides a highly accurate means to titrate radiofrequency ablation lesion depth," *J. Cardiovasc. Electrophysiol.*, vol. 22, pp. 684–690, 2011.

[15] M. Hayashi, "Temperature-electrical conductivity relation of water for environmental monitoring and geophysical data inversion," *Environ. Monitoring Assessment*, vol. 96, pp. 119–128, 2004.

[16] B. Avitall, K. Mughal, J. Hare, R. Helms, and D. Krum, "The effects of electrode-tissue contact on radiofrequency lesion generation," *Pacing Clin. Electrophysiol.*, vol. 20, pp. 2899–2910, 1997.

[17] E. Hoffmann, R. Haberl, R. Pulter, M. Gokel, and G. Steinbeck, "Biophysical parameters of radiofrequency catheter ablation," *Int. J. Cardiol.*, vol. 37, pp. 213–222, 1992.

[18] X. Zheng, G. P. Walcott, J. A. Hall, D. L. Rollins, W. M. Smith, G. N. Kay, and R. E. Ideker, "Electrode impedance: An indicator of electrode-tissue contact and lesion dimensions during linear ablation," *J. Interventional Card. Electrophysiol.*, vol. 4, pp. 645–654, 2000.

[19] N. Stagegaard, H. H. Petersen, X. Chen, and J. H. Svendsen, "Indication of the radiofrequency induced lesion size by pre-ablation measurements," *Europace*, vol. 7, pp. 525–534, 2005.

[20] M. E. Ring, S. K. Huang, G. Gorman, and A. R. Graham, "Determinants of impedance rise during catheter ablation of bovine myocardium with radiofrequency energy," *Pacing Clinical Electrophysiol.*, vol. 12, pp. 1502–1513, 1989.

[21] W. M. Hartung, M. E. Burton, A. G. Deam, P. F. Walter, K. McTeague, and J. J. Langberg, "Estimation of temperature during radiofrequency catheter ablation using impedance measurements," *Pacing Clin. Electrophysiol.*, vol. 18, pp. 2017–2021, 1995.

[22] J. Seiler, K. C. Roberts-Thomson, J. M. Raymond, J. Vest, E. Delacretaz, and W. G. Stevenson, "Steam pops during irrigated radiofrequency ablation: Feasibility of impedance monitoring for prevention," *Heart Rhythm*, vol. 5, pp. 1411–1416, 2008.

[23] D. Schwartzman, I. Chang, J. J. Michele, M. S. Mirotznik, and K. R. Foster, "Electrical impedance properties of normal and chronically infarcted left ventricular myocardium," *J. Interventional Card. Electrophysiol.*, vol. 3, pp. 213–224, 1999.

[24] M. Warren, R. Bragos, O. Casas, A. Rodriguez-Sinovas, J. Rosell, I. Anivarro, and J. Cinca, "Percutaneous electrocatheter technique for online detection of healed transmural myocardial infarction," *Pacing Clinical Electrophysiol.*, vol. 23, pp. 1283–1287, 2000.

[25] T. Gaspar, H. Sih, G. Hindricks, C. Eitel, P. Sommer, S. Kircher, S. Rolf, A. Arya, L. Teplitsky, and C. Piorkowski, "Use of electrical coupling information in AF catheter ablation: A prospective randomized pilot study," *Heart Rhythm*, vol. 10, pp. 176–181, 2013.

[26] D. Demazumder and D. Schwartzman, "Titration of radiofrequency energy during endocardial catheter ablation," in *Catheter Ablation of Cardiac Arrhythmias*, S. K. S. Huang and M. A. Wood, Eds. Philadelphia, PA, USA: Saunders Elsevier, 2006, pp. 21–34.

D. Curtis Deno (M'76) received the B.S.E.E. and M.S. degrees in biomedical engineering from Rensselaer Polytechnic Institute, Troy, NY, USA, the M.D. degree from Hahnemann University, Philadelphia, PA, USA, and the Ph.D. degree in electrical engineering and computer science from the University of California, Berkeley, CA, USA.

He has been engaged in medical device research and development for 21 years and is currently a Senior Principal Scientist with St. Jude Medical, St. Paul, MN, USA.

Haris J. Sih received the bachelor's degree from Massachusetts Institute of Technology, Cambridge, MA, USA, and the Master's and Doctoral degrees from Northwestern University, Evanston, IL, USA, all in electrical engineering.

From 1995 to 2000, he was a Visiting Assistant Professor at Indiana University – Purdue University Indianapolis, Indianapolis, IN, USA. He is currently a Principal Clinical Scientist with St. Jude Medical, St. Paul, MN, USA.

Stephan P. Miller received the B.S.M.E. degree in 1999 and the M.B.A. degree in 2006 from the University of Minnesota, Twin Cities, Minneapolis, MN, USA.

He has held positions in manufacturing engineering, research and development, and program management over 13 years at St. Jude Medical, St. Paul, MN, USA.

Liane R. Teplitsky received the Bachelor's degrees in electrical engineering and in physiology from the University of Saskatchewan, Saskatoon, Saskatchewan, Canada. She received the Master's degree in biomedical engineering from Duke University, Durham, NC, USA.

For the past 13 years, she has been engaged in many areas of the medical device industry from research and development to sales and marketing.

Russ Kuenzi received the B.S.E.E. degree from the University of Wisconsin, Madison, MI, USA, and the M.S.E.E. degree from the University of Minnesota, Twin Cities, Minneapolis, MN, USA.

He is presently a Senior Firmware Engineer with Cardiocom, Chanhassen, MN, USA, interested in analog and digital design, embedded firmware, and robotics.